

Layered Electrides as Fluoride Intercalation Anodes

Steven T. Hartman,^{†,⊥} and Rohan Mishra^{‡,†,}*

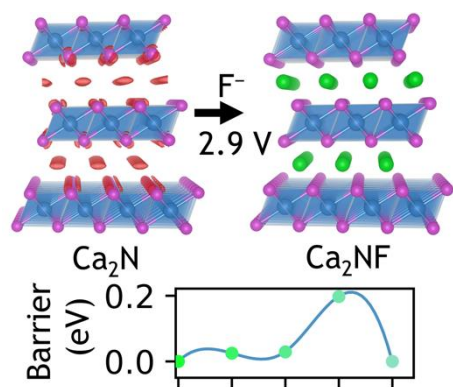
[†]Institute of Materials Science and Engineering, Washington University in St. Louis, One Brookings
Drive, St. Louis, MO 63130, USA

[‡]Department of Mechanical Engineering and Materials Science, Washington University in St. Louis, One
Brookings Drive, St. Louis, MO 63130, USA

*Email: S.T.H. (steven.t.hartman@wustl.edu) or R.M. (rmishra@wustl.edu)

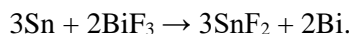
ABSTRACT: The fluoride ion is well suited to be the active species of rechargeable batteries, due to its small size, light weight, and high electronegativity. While existing F-ion batteries based on conversion chemistry suffer from rapid electrode degradation with cycling, those based on fluoride intercalation are currently less attractive than cation intercalation battery chemistries due to their low reversible energy densities. Here, using first-principles density-functional-theory calculations, we predict that layered electrides, such as Ca_2N and Y_2C — that have an electron occupying a lattice site — are promising hosts for fluoride intercalation, since their anionic electrons create large interstices. Our calculations indicate that anodes made from layered electrides can offer voltage up to -2.86 V vs. La_2CoO_4 cathode, capacity >250 mAh/g, and fast diffusion kinetics with migration barriers as low as 0.15 eV. These metrics compare favorably to popular Li-ion intercalation cathodes such as LiCoO_2 . Electrides open up a new space for designing fluorine intercalation batteries with good performance and cyclability.

TOC GRAPHIC



Rechargeable batteries enable crucial modern technologies, such as mobile phones, electric cars, and aerial drones, and will be required in even larger numbers for the rapidly growing automotive fleets and grid-scale storage of electricity generated by intermittent renewable sources. Currently, the market is dominated by Li-ion batteries, which shuttle lithium ions between two intercalation electrodes such as graphite and LiCoO₂. In these electrodes, the Li ions move into empty spaces in a host material without significantly disrupting the host's structure. While this design has achieved high energy density and adequate cycling stability, the supply risk of lithium and cobalt¹ is predicted to create obstacles for the surge in battery usage. Current Li-ion batteries also pose safety concerns due to Li dendrite growth and thermal runaway.² Therefore, it is desirable to find other high-performance battery chemistries besides Li-ion.

The search for alternative chemistries has primarily been limited to light cations such as Na⁺,³ K⁺,⁴ Mg²⁺,⁵ Zn²⁺,⁶ and Al³⁺.⁷ A handful of studies have instead focused on using anions as the active species.^{8,9} Amongst the various candidates for active anion batteries, fluoride (F⁻) is especially attractive due to its earth-abundance, light weight, high electronegativity, and reasonably fast diffusion in liquid or solid electrolytes.¹⁰⁻¹⁷ In contrast to the success of Li batteries using two intercalation electrodes, most research on fluoride-ion batteries (FiBs) has followed a different path involving conversion reactions,^{18,19} pairing metals with metal fluorides, such as:¹¹



The theoretical current capacity of conversion electrodes can be very high, such as 669 mAh/g for Ca/CaF₂, compared to 294 mAh/g for LiCoO₂. However, these high capacities are difficult to achieve in practice. The phase transformation of the metal to its fluoride during charge/discharge cycles is typically a slow reaction which requires a large overpotential; furthermore, if the resulting volume change is large, the electrode can crumble and degrade during repeated cycling.²⁰ In addition, the pure metal electrode sometimes dissolves into the electrolyte, further degrading it.¹⁹ These effects are also seen in Li-ion conversion batteries, which have not found commercial success despite extensive research.²¹ Therefore, prior experience suggests the value of intercalation FiBs, but high-capacity, fluoride intercalation

electrodes have not been reported. The first F^- intercalation electrode to be tested was $LaSrMnO_4/LaSrMnO_4F_2$,¹³ which offered a moderate theoretical capacity of 172 mAh/g, but proved to have very limited reversibility due to destructive side reactions and overpotentials >1 V. La_2CoO_4/La_2CoO_4F later provided improved cycling durability, but at the cost of low theoretical capacity (67 mAh/g).^{18, 22} These electrodes have relatively little driving force for fluoride intercalation, making them suitable for cathodes, while FiB intercalation anodes have not yet been demonstrated.

In this Article, we take a new approach to design intercalation $FiBs$, which is to use the unconventional chemistry of electride crystals to our advantage. These inorganic electrides have interstices occupied by free electrons that act as anions, due to their unusual stoichiometries, which are not charge-balanced in common oxidation states.²³ We use first-principles density-functional-theory (DFT) calculations to show that electrides can intercalate fluoride stably by replacing the free electron with a F^- . Among the 12 known or predicted electrides which we have examined, we predict Ca_2N and Y_2C as promising candidates for intercalation anodes with theoretical gravimetric capacities ~ 280 mAh/g, volume change during cycling $<15\%$, voltage <-2.5 V vs. La_2CoO_4 cathode, and low kinetic barriers <0.2 eV for fluoride ion transport. These values approach the performance of popular Li-ion electrodes such as $LiCoO_2$, which has a theoretical capacity 295 mAh/g, calculated voltage 3.7 V vs. graphite, and migration barriers ~ 0.3 eV,²⁴ and Ca_2N in particular is much more earth-abundant than $LiCoO_2$. The excellent performance metrics of Ca_2N and Y_2C , if realized experimentally, will be a major step toward the practical use of $FiBs$.

First, we consider the crystal structures of Li-intercalation electrodes, to see if the proven design principles can be transferred directly to $FiBs$. Two of the most successful Li^+ intercalation cathodes, $LiFePO_4$ ²⁵ and $LiCoO_2$,²⁶ are shown in Figures 1a and b, respectively. They are characterized by anionic polyhedra that are centered on small, highly charged cations (Shannon radius of 0.65 Å for Fe^{3+} , 0.17 Å for P^{5+} , and 0.53 Å for Co^{4+}). The Li^+ ions rest in the interstices between these polyhedra. The transition metal ions, besides providing the redox activity by changing their oxidation state, also serve to hold the crystal together when the Li^+ is absent (in the charged state). Thanks to these framework-preserving

cations, LiCoO_2 and LiFePO_4 have calculated volume changes of only 3% and 7 %, ²⁴ respectively, as Li is removed, promoting durability over many cycles.

Based on these examples, to intercalate F^- , we ought to invert the paradigm and have cationic polyhedra centered on some other anion, to maintain the structural integrity in the absence of F^- ions. However, we immediately notice that anions are generally larger than cations, ²⁷ with F^- having the smallest Shannon radius of 1.33 Å. In addition to making fluoride intercalation more challenging, the large size of anions also restricts the construction of anion-centered polyhedra. Therefore, the best candidates for anion-centered polyhedra are the first-row species N^{3-} (1.46 Å), B^{3-} , C^{4-} , and possibly O^{2-} (1.4 Å). ^{28, 29} As for the surrounding cations, they should be large enough to create stable polyhedra with spacious interstices between them. They should also have a low charge to achieve charge balance, since they are more numerous than the central anion even if the polyhedra share many edges and faces. The cation also needs to be light for good gravimetric capacity, and inexpensive. Finally, it ought to be redox-active, with several stable oxidation states.

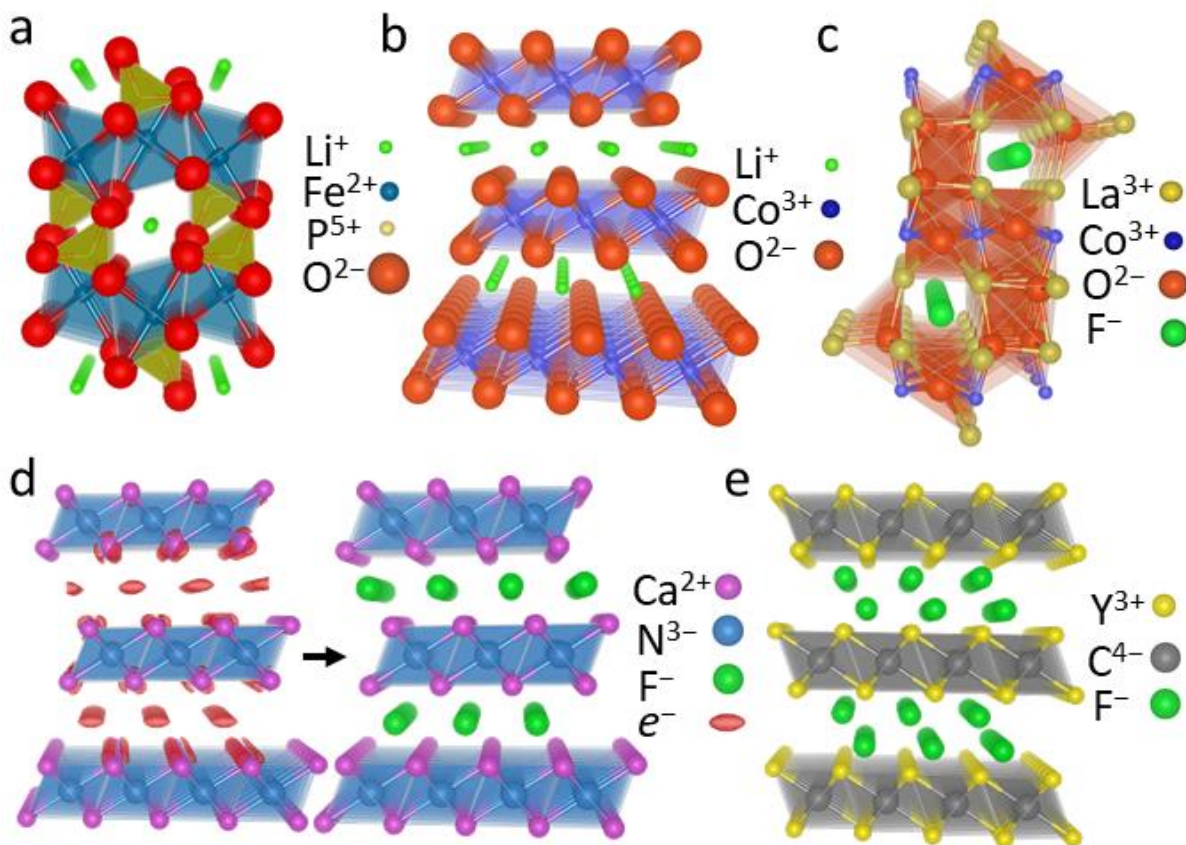
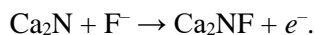


Figure 1. Structural principles for fluorine intercalation electrode design. **a.** The popular Li-ion intercalation electrode LiFePO_4 , in which Li^+ (green) occupies distorted octahedral sites between PO_4 tetrahedra and FeO_6 distorted octahedra. **b.** LiCoO_2 , with Li^+ sitting in octahedral interstices between layers of edge-sharing CoO_6 octahedra. **c.** The previously known F^- intercalation electrode $\text{La}_2\text{CoO}_4\text{F}$, with F^- (green) in tetrahedral interstices between strongly distorted La_5CoO octahedra. **d.** The newly proposed Ca_2NF electrode, with F^- in octahedral interstices between layers of edge-sharing Ca_6N octahedra. The localized electrons between the Ca_2N layers are shown with isosurfaces of the electron localization function. Ca_2NF 's structure is the inverse of LiCoO_2 's structure in **b.** **e.** Y_2CF_2 , with F^- in tetrahedral interstices between layers of edge-sharing Y_6C octahedra.

These constraints are not easily satisfied by a single cation, and indeed all existing fluoride intercalation electrodes combine two or more cation species. Figure 1c shows the most successful electrode to date, $\text{La}_2\text{CoO}_4\text{F}$,^{18, 22} which uses the larger La^{3+} cations (1.16 Å) to create large tetrahedral sites for F^- in the rock-salt structured LaO layers. The smaller Co^{2+} (0.65 Å) occupies CoO_2 layers which provide the redox activity, as F^- intercalation onto the LaO layers oxidizes Co to 3+. However, the gravimetric capacity is low (67 mAh/g theoretically) because the heavy La is “dead weight” from an electrochemical perspective.

This is generally true for similar electrodes such as $\text{MgFeSb}_4\text{O}_8\text{F}$ (39 mAh/g) or $\text{CoFeSb}_4\text{O}_8\text{F}$ (37 mAh/g),³⁰ although it can be mitigated by using cations lighter than La or Sb, such as Sr (1.26 Å) in $\text{Sr}_2\text{TiO}_3\text{F}_2$ (197 mAh/g), which has been proposed as a FiB anode but not yet tested.³¹

We conclude that to keep the electrode light, yet retain large interstitial sites, it should ideally have only one type of cation. Alkali and alkaline earth metals are light, large, inexpensive, and have low charge, satisfying all the constraints except redox activity, so we can expect good results if these metals can be stabilized in oxidation states besides +1 and +2, respectively. Such materials are rare, but a small group of suboxides, subnitrides, and hypocarbides are stable with fewer anions than would be expected by charge balance.³² One well-studied example is the electride Ca_2N , which from a chemical perspective can be represented as $\text{Ca}_2^{2+}\text{N}^{3-}e^-$, where e^- is an electron localized at an empty anion site. We show the structure of Ca_2N in Figure 1d. Ca_2N has an inverse LiCoO_2 structure, with Ca_6N octahedra instead of CoO_6 , and Li replaced by anionic electrons. This suggests the following half-reaction can proceed topochemically, with little volume change:



While Ca_2N is referenced as a possible FiB electrode in a patent application,³³ any related studies remain unpublished, so a detailed theoretical study offers the first opportunity to understand the F^- intercalation properties of Ca_2N .

To assess the intercalation of Ca_2N with F^- ions, we have calculated the stability of the products and reactants for a variety of fluoride intercalation reactions along with the associated change in voltage and volume using DFT. For details of these calculations, see the section on Computational Methods. We find that both Ca_2N and Ca_2NF , with their structures shown in Figure 1d, are on the convex hull, and hence, stable against decomposition into known competing phases present in the Materials Project database.²⁴ The fluoride ion occupies the octahedral site between Ca_2N layers, while the tetrahedral sites, which are twice as many as the octahedral sites, are unoccupied. Placing fluoride into the tetrahedral site costs 0.34 eV more than the octahedral site. Upon geometry optimization, we find that Ca_2NF retains the same

rhombohedral $R\bar{3}m$ phase as Ca_2N . For this structure, we can calculate its gravimetric capacity to be 285 mAh per gram of Ca_2N according to Eqn. 1:

$$\frac{1 \text{ mol } \text{Ca}_2\text{N}}{94 \text{ g } \text{Ca}_2\text{N}} \times \frac{1 \text{ mol } e^-}{1 \text{ mol } \text{Ca}_2\text{N}} \times \frac{96485 \text{ A} \times \text{s}}{1 \text{ mol } e^-} \times \frac{1000 \text{ mA}}{1 \text{ A}} \times \frac{1 \text{ h}}{3600 \text{ s}} = \frac{285 \text{ mAh}}{1 \text{ g}}. \quad [1]$$

We note that while Ca_2NCl and Ca_2NBr are experimentally reported to exist in the $R\bar{3}m$ phase,^{34, 35} Ca_2NF has only been made in the $I4_1/amd$ phase,³⁶ which we find is 5 meV/atom higher in energy than the $R\bar{3}m$ phase. Therefore, we expect that low-temperature fluorination, which has emerged as a successful strategy to produce fluoride structures topochemically,^{37, 38} should yield $R\bar{3}m$ Ca_2NF from $R\bar{3}m$ Ca_2N . The $R\bar{3}m$ phase's volume shrinks 13% during fluorination, and the electromotive force is -2.86 V vs. $\text{La}_2\text{CoO}_4/\text{La}_2\text{CoO}_4\text{F}$, calculated with:

$$\frac{E_{\text{Ca}_2\text{NF}} + E_{\text{La}_2\text{CoO}_4} - E_{\text{Ca}_2\text{N}} - E_{\text{La}_2\text{CoO}_4\text{F}}}{1} = -2.86 \text{ V}, \quad [2]$$

where $E_{\text{Ca}_2\text{NF}}$ and $E_{\text{La}_2\text{CoO}_4}$ are the calculated energies of the products, $E_{\text{Ca}_2\text{N}}$ and $E_{\text{La}_2\text{CoO}_4\text{F}}$ are the energies of the reactants, and 1 is the number of electrons transferred in the reaction. -2.86 V is the same calculated potential as the Li/LiF half-reaction, indicating that Ca_2N is highly electropositive, consistent with its experimentally known sensitivity to air and moisture.³⁹ Ca_2NF can be further fluorinated to Ca_2NF_2 at -0.78 V vs. $\text{La}_2\text{CoO}_4/\text{La}_2\text{CoO}_4\text{F}$, but we do not include this in its theoretical capacity, since it is not clear if the anion-redox capacity is accessible without degrading the electrode. The Ca_2NF_2 phase is 237 meV/atom above the Materials Project convex hull, excluding species such as CaN_6 which are poorly described by DFT,⁴⁰ and it might decompose by nitrogen gas evolution to produce Ca_2NF and CaF_2 .

Another electride isostructural to Ca_2N , Y_2C ,⁴¹ is also a promising candidate for FiB anodes. Y_2C , as shown in Figure 1e, can be represented as $\text{Y}_2^{3+}\text{N}^{3-}2e^-$ with $2e^-$ nominally residing at the octahedral sites. Recently, Druffel et al. reported the formation of Y_2CF_2 using a high-temperature solid-state reaction of Y , YF_3 , and graphite.⁴² F^- ions are observed to occupy the tetrahedral sites between the Y_2C layers of Y_2CF_2 , and the Y_2C layers re-stack from their original ABC stacking pattern to an AAA stacking in Y_2CF_2 with space group $P\bar{3}m1$, as shown in Figure 1e. As a consequence of the AAA stacking, we find that

Y_2CF_2 expands by 9% in volume relative to Y_2C , in good agreement with the 8% volume change found experimentally. We also calculate the fluorination voltage to be -2.56 V vs. $\text{La}_2\text{CoO}_4/\text{La}_2\text{CoO}_4\text{F}$, and a gravimetric capacity of 282 mAh/g.

The intermediate Y_2CF phase, with F^- in octahedral sites, is unstable by 81 meV/atom with respect to Y_2C and Y_2CF_2 , indicating that Y_2C is likely to fluorinate in a one-step process without staging. Further evidence for a one-step reaction is provided by the formation energy of the neutral F^- vacancy, which we calculate to be 0.14 eV at the chemical potential defined by the $\text{Y}_2\text{C}/\text{Y}_2\text{CF}_2$ equilibrium. Creating two adjacent fluoride vacancies costs 0.46 eV. Neglecting entropy, it is easier to defluorinate Y_2CF_2 all at once, than to remove one or two F^- at a time. Most Li-ion batteries discharge in stages because the electrostatic repulsion between Li^+ gradually reduces the driving force to insert additional Li^+ ,⁴³ but the empty octahedral F^- sites of the electrides can still be occupied by a negatively charged electron, so an electrostatic repulsion still occurs in the empty state. We have calculated the electrostatic interactions using VESTA,⁴⁴ assuming that all anionic free electrons are localized in the octahedral interstitial site. Y_2CF_2 has a total Madelung energy of -174 eV/f.u., compared to -185 eV/f.u. for Y_2C . This includes the contribution of the re-stacking; Ca_2NF does not re-stack, and has a Madelung energy of -89.5 eV/f.u., much closer to the -87.8 eV/f.u. of Ca_2N . As a comparison, the Madelung energy of LiCoO_2 is -110 eV/f.u. and that of CoO_2 is -140 eV/f.u..

Based on these thermodynamic calculations, we expect the layered electrides to have good energy storage capacity, but the diffusion kinetics are also important. To achieve high power density, a battery electrode must conduct the active ion rapidly. Since the layered structures of Ca_2NF and Y_2CF_2 match LiCoO_2 so closely, it is reasonable to expect them to have fast two-dimensional ion transport kinetics, which we calculate using the climbing-image nudged elastic-band (NEB) technique.⁴⁵ To provide a benchmark, we first examine the vacancy diffusion mechanism of the known cathode material $\text{La}_2\text{CoO}_4\text{F}$, which is shown in Figure 2a, with a barrier to fluoride migration of 0.83 eV. For the layered electrides, we consider three mechanisms: vacancy-assisted diffusion, direct interstitial diffusion, and interstitialcy (kick-out) diffusion. The lowest barrier for Ca_2NF is the interstitialcy diffusion mechanism with a barrier

of 0.2 eV. Y_2CF_2 is more likely to exhibit vacancy diffusion with a barrier of 0.16 eV. Both of these barriers compare favorably to the calculated barrier of 0.2-0.3 eV for LiCoO_2 .⁴⁶

The NEB barriers assume the existence of an empty defect site (interstitial for Ca_2NF and F-vacancy for Y_2CF_2), but the total activation energy E_A for diffusion is the formation energy of the relevant electrically neutral defect, plus the kinetic barrier height. When calculating the formation energy of the defects, we can assume either fluorine-rich and fluorine-poor conditions, which are the fluoride chemical potentials required to defluorinate or further fluorinate the electride. In Ca_2NF , the dominant mechanism switches from interstitialcy to vacancy diffusion when the

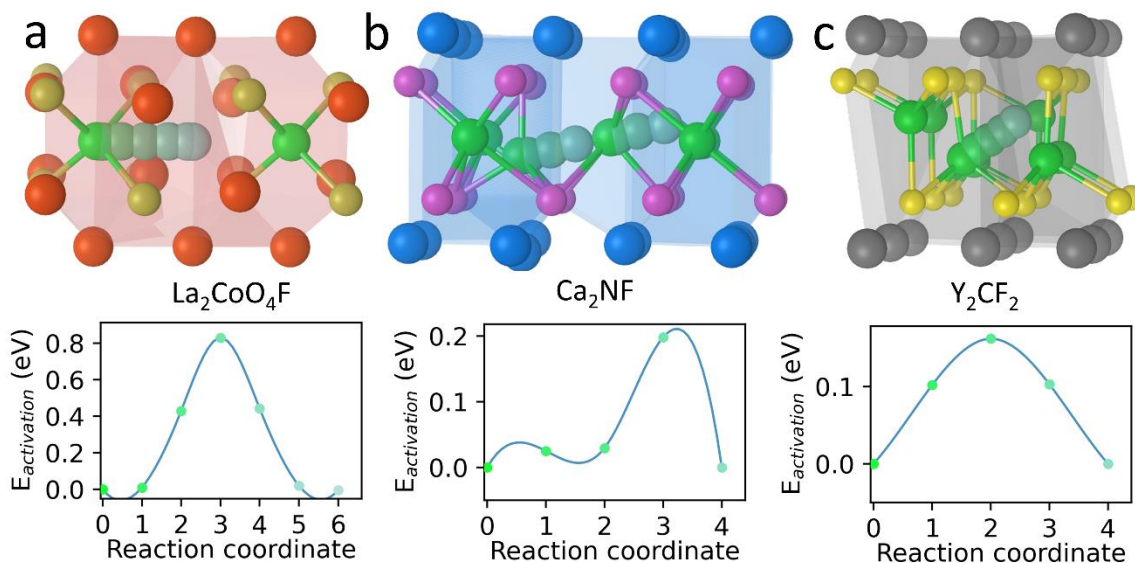


Figure 2: NEB study of F^- diffusion kinetics. **a.** Vacancy diffusion in $\text{La}_2\text{CoO}_4\text{F}$. A tetrahedral F^- moves to an adjacent vacant tetrahedral site in the LaO layer. The plot shows the diffusion barrier for the motion of F^- . **b.** Interstitialcy mechanism in Ca_2NF . A tetrahedral F^- interstitial displaces an octahedral F^- , which moves to a tetrahedral interstitial site on the opposite side as the original. **c.** Vacancy diffusion mechanism in Y_2CF_2 . A tetrahedral F^- moves to an adjacent tetrahedral site.

fluoride chemical potential is reduced, because the fluoride interstitial costs 2.3 eV to form under fluoride-poor conditions while the F^- vacancy only costs 0.3 eV. In contrast, we predict that Y_2CF_2 favors vacancy diffusion under any stable fluoride potential, since the F^- vacancy's formation energy never exceeds 0.5 eV. The total calculated activation energies are 1.61-1.64 eV for Ca_2NF and 0.30-0.71 eV for

Y_2CF_2 , indicating that Y_2CF_2 is likely to have much faster kinetics. We estimate the diffusivity D using Eqn. 3:⁴⁶

$$D = \frac{l^2 v_0}{2n} \exp\left(-\frac{E_A}{kT}\right). \quad [3]$$

Here the dimensionality $n = 2$, l is the length of a single jump, k is the Boltzmann constant, and we approximate the attempt frequency v_0 as $v_0 = 10^{13}/\text{s}$. We obtain a negligible value of $D = 2.4 \times 10^{-30} \text{ cm}^2/\text{s}$ for Ca_2NF at 298 K and F-poor conditions, while Y_2CF_2 has $D = 1.4 \times 10^{-8} \text{ cm}^2/\text{s}$. Sample characteristics such as grain size will also influence the experimental diffusivity.⁴⁷ Because Ca_2NF 's interstitialcy diffusion has a low kinetic barrier height $< 0.2 \text{ eV}$, we expect the diffusion can be enhanced by extrinsic doping, such as with Y^{3+} , to increase F^- interstitial concentration.

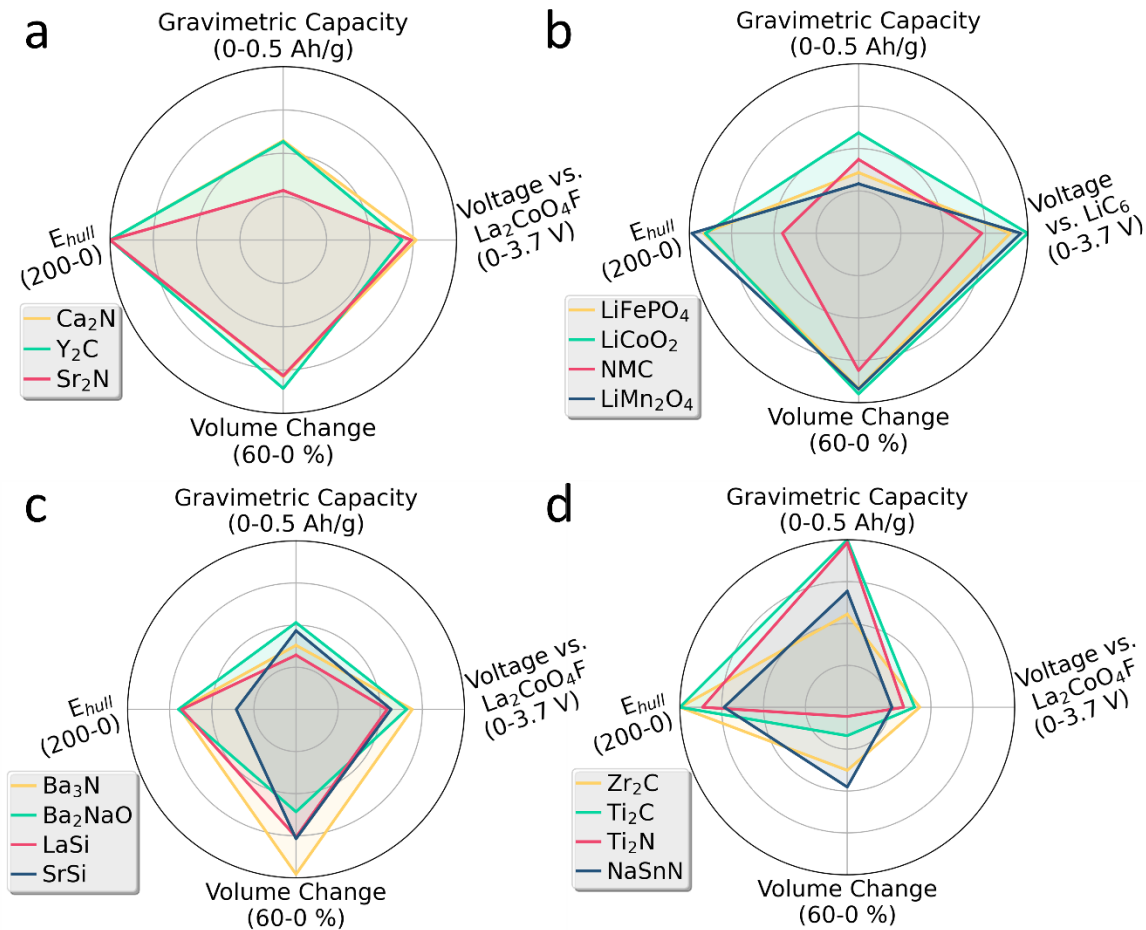


Figure 3: Comparison of structural families for intercalation electrodes. Gravimetric capacity and voltage are normalized with respect to the highest score in each category. The voltage is the average voltage for the complete reaction with $\text{La}_2\text{CoO}_4\text{F}$ or LiC_6 , not accounting for any steps in the voltage profile. Thermodynamic stability is measured with the hull energy E_{hull} , in meV/atom, of whichever electrode state (charged or discharged) is less stable, and plotted from 200 meV above the hull to 0. Likewise, the magnitude of the volume change of the intercalated phase with respect to the de-intercalated phase is plotted from 60% to 0%. Calculated data for these and other electrodes are in Supporting Information. **a.** The layered electrides which are the focus of this work. **b.** Commercially successful Li-ion battery cathodes, for comparison. **c.** Other predicted electrides with different structures than Ca_2N . **d.** 2D mxenes, and the closely related material NaSnN .

While Ca_2N and Y_2C are the most promising electrides for use in FiBs identified in this study, we have also calculated the F^- intercalation properties of several other electrides, including LaSi , SrSi , Ba_3N , and Ba_2NaO ,⁴⁸⁻⁵⁰ for comparison. In addition, we have calculated the stability and capacity of several known MXenes,²⁹ which are structurally related to the layered electrides, although their chemical properties are different. We compare the theoretical performance of these different structural families in Figure 3, with popular Li-ion electrodes shown as a reference. Ca_2N and Y_2C have calculated performances closest to that of their structural analogue LiCoO_2 , with excellent thermodynamic stability and current capacity. The other electrides are not as promising, since their structures do not allow fluoride intercalation with the same stability as the layered electrides. However, the structure alone is not enough without the electride chemistry. The isostructural MXenes have high gravimetric capacity — up to 497 mAh/g for Ti_2C — due to their light weight, but also have low voltage and experience large volume changes. The electride chemistry turns out to be essential because the free anionic electrons have a very low work function ~ 2.5 eV,⁵¹ the same as Li metal.⁵² Because electrides give up electrons easily, they have a higher voltage vs. the cathode. The anionic electrons also improve the cycling stability by acting in combination with the large Ca^{2+} and Y^{3+} cations to maintain large interstices even in the unfluorinated state.

Our calculations suggest that Ca_2N and Y_2C can perform very well as FiB anodes. Going forward, there are several other FiB components which require improvement for these anodes to be used at their full capability. The most important target for further research is the voltage stability window of the electrolyte and a conductive additive. Ca_2N is likely to form a solid-electrolyte interphase (SEI) in contact with solid

fluoride electrodes such as $\text{La}_{1-x}\text{Ba}_x\text{F}_{3-x}$ (LBF), since Li/LiF has the same potential of -2.86 V and is known to reduce LBF,⁵³ while Y_2C is right on the edge of the stability window. The effect of this SEI is not yet known, and it might be preferable to find an electrolyte which is stable against Ca_2N . At the other end of the voltage window, La_2CoO_4 is the highest-voltage practical cathode, at 2.86 V vs. $\text{Ca}_2\text{N}/\text{Ca}_2\text{NF}$. Higher-voltage cathodes are known, but at those voltages the commonly used conductive additive, carbon black, reacts irreversibly with F^- .^{13, 30, 53} The carbon fluorination may be avoided in the future through the introduction of improved conductors such as SnO_2 or carbon nanotubes.²⁰ In order to compete with Li-ion batteries, the accessible voltage range must be expanded to >3 V, and intercalation cathodes with higher capacities than La_2CoO_4 or LaSrMnO_4 are required.

In summary, we have calculated the properties of different FiB intercalation electrodes, and find that Ca_2N and Y_2C can offer an excellent combination of energy density, power density, and cycling stability. Their useful properties are due to the unique chemistry of layered electrides, which have free anionic electrons occupying vacant anion sites in the defluorinated state. Both materials intercalate F^- with very low kinetic barriers for F^- diffusion, and less volume change than most conversion electrodes, which is ideal for fast and reversible charge/discharge cycles. We expect that these new anodes will significantly advance FiBs' energy storage capability.

COMPUTATIONAL METHODS

We performed all DFT calculations using the VASP software,^{54, 55} and chose our calculation parameters to be compatible with the Materials Project database.^{24, 56} Certain calculations could not be converged using the tetrahedron method for electronic smearing, so these were completed using Gaussian smearing with a small SIGMA of 0.01, to minimize the discrepancy compared to the tetrahedron method. To maintain compatibility with the Materials Project, we did not include van der Waals corrections (see Supporting Information for tests of the effects of vdW corrections). All gravimetric capacities were calculated with respect to the mass of the defluorinated or delithiated state, and the reported voltage is the electromotive force driving the complete reaction, which does not include the “steps” seen in many

experimental discharge curves due to intermediate phases. The initial locations of fluoride atoms were selected manually, a procedure which is unambiguous for the layered electrides with their clearly defined octahedral and tetrahedral sites.

We used 3x3x1 supercells for the NEB calculations of Ca_2NF and Y_2CF_2 , which contained 81 atoms plus the added fluorine. Ionic positions were relaxed to a force convergence criterion of $0.02 \text{ eV}/\text{\AA}$, with two exceptions. The Y_2CF_2 interstitial diffusion was terminated after 200 steps because the F^- could not fit through the saddle point, and was taking an alternate route with very high energy. The saddle-point image of Ca_2NF 's interstitialcy mechanism was well-converged, but the first image could not be converged even after several hundred ionic steps. The fluorine-poor limit is defined by the $\text{Ca}_2\text{N}/\text{Ca}_2\text{NF}$ or $\text{Y}_2\text{C}/\text{Y}_2\text{CF}_2$ equilibrium, while the fluorine-rich limit is the $\text{Ca}_2\text{NF}/(2\text{CaF}_2 + 0.5\text{N}_2)$ or $\text{Y}_2\text{CF}_2/(2\text{YF}_3 + \text{C})$ equilibrium.

ASSOCIATED CONTENT

Supporting Information: Performance metrics of other anode materials investigated in this study; effect of van der Waals corrections.

AUTHOR INFORMATION

Corresponding author: *Email: S.T.H. (steven.t.hartman@wustl.edu) or R.M. (rmishra@wustl.edu).

Present Address: [†](S.T.H.) Materials Science and Technology Division, Los Alamos National Laboratory, Los Alamos, NM 87545, USA.

Conflicts of interest: The authors declare no competing financial interest.

ACKNOWLEDGMENTS

This work was supported by the National Science Foundation (NSF) grant numbers DMREF-1729787 and DMR-1806147. This work used computational resources of the Extreme Science and Engineering Discovery Environment (XSEDE), which is supported by NSF grant number ACI-1548562.

REFERENCES:

1. C. Helbig, A. M. Bradshaw, L. Wietschel, A. Thorenz and A. Tuma, *Journal of Cleaner Production*, 2018, **172**, 274-286.
2. D. H. Dougherty and E. P. Roth, *The Electrochemical Society Interface*, 2012, **21**, 37-44.
3. N. Yabuuchi, K. Kubota, M. Dahbi and S. Komaba, *Chemical Reviews*, 2014, **114**, 11636-11682.
4. J. C. Pramudita, D. Sehwat, D. Goonetilleke and N. Sharma, *Advanced Energy Materials*, 2017, **7**, 1602911.
5. J. Song, E. Sahadeo, M. Noked and S. B. Lee, *The Journal of Physical Chemistry Letters*, 2016, **7**, 1736-1749.
6. D. Kundu, B. D. Adams, V. Duffort, S. H. Vajargah and L. F. Nazar, *Nature Energy*, 2016, **1**, 16119.
7. N. Jayaprakash, S. K. Das and L. A. Archer, *Chemical Communications*, 2011, **47**, 12610-12612.
8. X. Zhao, S. Ren, M. Bruns and M. Fichtner, *Journal of Power Sources*, 2014, **245**, 706-711.
9. X. Zhao, Z. Zhao-Karger, M. Fichtner and X. Shen, *Angewandte Chemie International Edition*, 2019, **0**.
10. M. Oka, H. Kamisaka, T. Fukumura and T. Hasegawa, *Computational Materials Science*, 2019, **167**, 92-99.
11. I. Mohammad, R. Witter, M. Fichtner and M. Anji Reddy, *ACS Applied Energy Materials*, 2018, DOI: 10.1021/acsaem.8b00864.
12. V. K. Davis, C. M. Bates, K. Omichi, B. M. Savoie, N. Momčilović, Q. Xu, W. J. Wolf, M. A. Webb, K. J. Billings, N. H. Chou, S. Alayoglu, R. K. McKenney, I. M. Darolles, N. G. Nair, A. Hightower, D. Rosenberg, M. Ahmed, C. J. Brooks, T. F. Miller, R. H. Grubbs and S. C. Jones, *Science*, 2018, **362**, 1144.
13. M. A. Nowroozi, K. Wissel, J. Rohrer, A. R. Munnangi and O. Clemens, *Chemistry of Materials*, 2017, **29**, 3441-3453.
14. F. Gschwind, G. Rodriguez-Garcia, D. J. S. Sandbeck, A. Gross, M. Weil, M. Fichtner and N. Hörmann, *Journal of Fluorine Chemistry*, 2016, **182**, 76-90.
15. F. Gschwind and J. Bastien, *Journal of Materials Chemistry A*, 2015, **3**, 5628-5634.
16. C. Rongeat, M. Anji Reddy, R. Witter and M. Fichtner, *ACS Applied Materials & Interfaces*, 2014, **6**, 2103-2110.
17. M. Anji Reddy and M. Fichtner, *Journal of Materials Chemistry*, 2011, **21**, 17059-17062.
18. M. A. Nowroozi and O. Clemens, *ACS Applied Energy Materials*, 2018, DOI: 10.1021/acsaem.8b01630.
19. D. T. Thieu, M. H. Fawey, H. Bhatia, T. Diemant, V. S. K. Chakravadhanula, R. J. Behm, C. Kübel and M. Fichtner, *Advanced Functional Materials*, 2017, **27**, 1701051.
20. L. Zhang, M. A. Reddy and M. Fichtner, *Journal of Solid State Electrochemistry*, 2018, **22**, 997-1006.
21. A. Kraytsberg and Y. Ein-Eli, *Journal of Solid State Electrochemistry*, 2017, **21**, 1907-1923.
22. M. A. Nowroozi, S. Ivlev, J. Rohrer and O. Clemens, *Journal of Materials Chemistry A*, 2018, **6**, 4658-4669.
23. K. Lee, S. W. Kim, Y. Toda, S. Matsuishi and H. Hosono, *Nature*, 2013, **494**, 336-340.
24. A. Jain, S. P. Ong, G. Hautier, W. Chen, W. D. Richards, S. Dacek, S. Cholia, D. Gunter, D. Skinner, G. Ceder and K. A. Persson, *APL Materials*, 2013, **1**, 011002.

25. A. K. Padhi, K. S. Nanjundaswamy and J. B. Goodenough, *Journal of The Electrochemical Society*, 1997, **144**, 1188-1194.
26. K. Mizushima, P. C. Jones, P. J. Wiseman and J. B. Goodenough, *Materials Research Bulletin*, 1980, **15**, 783-789.
27. R. Shannon, *Acta Crystallographica Section A*, 1976, **32**, 751-767.
28. S. V. Krivovichev, O. Mentré, O. I. Siidra, M. Colmont and S. K. Filatov, *Chemical Reviews*, 2013, **113**, 6459-6535.
29. M. Naguib, V. N. Mochalin, M. W. Barsoum and Y. Gogotsi, *Advanced Materials*, 2014, **26**, 992-1005.
30. M. A. Nowroozi, B. de Laune and O. Clemens, *ChemistryOpen*, 2018, **7**, 617-623.
31. K. Wissel, S. Dasgupta, A. Benes, R. Schoch, M. Bauer, R. Witte, A. D. Fortes, E. Erdem, J. Rohrer and O. Clemens, *Journal of Materials Chemistry A*, 2018, DOI: 10.1039/C8TA01012A.
32. A. Simon, *Coordination Chemistry Reviews*, 1997, **163**, 253-270.
33. K. Omichi, Q. Xu and C. Brooks, *Journal*, 2019.
34. C. Hadenfeldt and H. Herdejürgen, *Zeitschrift für anorganische und allgemeine Chemie*, 1987, **545**, 177-183.
35. A. Bowman, P. V. Mason and D. H. Gregory, *Chemical Communications*, 2001, DOI: 10.1039/B105448C, 1650-1651.
36. R. A. Nicklow, T. R. Wagner and C. C. Raymond, *Journal of Solid State Chemistry*, 2001, **160**, 134-138.
37. K. Wissel, J. Heldt, P. B. Groszewicz, S. Dasgupta, H. Breitzke, M. Donzelli, A. I. Waidha, A. D. Fortes, J. Rohrer, P. R. Slater, G. Buntkowsky and O. Clemens, *Inorg. Chem.*, 2018, DOI: 10.1021/acs.inorgchem.8b00661.
38. O. Clemens and R. Slater Peter, *Journal*, 2013, **33**, 105.
39. E. T. Keve and A. C. Skapski, *Chemical Communications (London)*, 1966, DOI: 10.1039/C19660000829, 829-830.
40. W. Sun, S. T. Dacek, S. P. Ong, G. Hautier, A. Jain, W. D. Richards, A. C. Gamst, K. A. Persson and G. Ceder, *Science Advances*, 2016, **2**.
41. M. Atoji and M. Kikuchi, *The Journal of Chemical Physics*, 1969, **51**, 3863-3872.
42. D. L. Druffel, M. G. Lanetti, J. D. Sundberg, J. T. Pawlik, M. S. Stark, C. L. Donley, L. M. McRae, K. M. Scott and S. C. Warren, *Chemistry of Materials*, 2019, DOI: 10.1021/acs.chemmater.9b03722.
43. A. Urban, D.-H. Seo and G. Ceder, *npj Computational Materials*, 2016, **2**, 16002.
44. K. Momma and F. Izumi, *J. Appl. Crystallogr.*, 2011, **44**, 1272-1276.
45. G. Henkelman, B. P. Uberuaga and H. Jónsson, *The Journal of Chemical Physics*, 2000, **113**, 9901-9904.
46. M. Okubo, Y. Tanaka, H. Zhou, T. Kudo and I. Honma, *The Journal of Physical Chemistry B*, 2009, **113**, 2840-2847.
47. L. N. Patro and K. Hariharan, *Solid State Ionics*, 2013, **239**, 41-49.
48. Q. Zhu, T. Frolov and K. Choudhary, *Matter*, 2019, DOI: <https://doi.org/10.1016/j.matt.2019.06.017>.
49. L. A. Burton, F. Ricci, W. Chen, G.-M. Rignanese and G. Hautier, *Chemistry of Materials*, 2018, **30**, 7521-7526.
50. T. Tada, S. Takemoto, S. Matsuishi and H. Hosono, *Inorganic Chemistry*, 2014, **53**, 10347-10358.

51. M. M. Menamparambath, J.-H. Park, H.-S. Yoo, S. P. Patole, J.-B. Yoo, S. W. Kim and S. Baik, *Nanoscale*, 2014, **6**, 8844-8851.
52. P. A. Anderson, *Physical Review*, 1949, **75**, 1205-1207.
53. A. Grenier, A. G. Porras-Gutierrez, M. Body, C. Legein, F. Chrétien, E. Raymundo-Piñero, M. Dollé, H. Groult and D. Dambournet, *The Journal of Physical Chemistry C*, 2017, **121**, 24962-24970.
54. G. Kresse and D. Joubert, *Physical Review B*, 1999, **59**, 1758-1775.
55. G. Kresse and J. Furthmuller, *Physical Review B*, 1996, **54**, 11169-11186.
56. S. P. Ong, W. D. Richards, A. Jain, G. Hautier, M. Kocher, S. Cholia, D. Gunter, V. L. Chevrier, K. A. Persson and G. Ceder, *Computational Materials Science*, 2013, **68**, 314-319.